Preprints.org

Article

Not peer-reviewed version

Structural and Luminescence Properties of Eu-Doped PMO Films with Ethylene Bridge and Methyl Terminal Groups

Md Rasadujjaman *, Jinming Zhang, Alexey S. Vishnevskiy, Jing Zhang *, Mikhail R. Baklanov

Posted Date: 31 July 2023

doi: 10.20944/preprints202307.2068.v1

Keywords: organosilica glass; europium; ethylene bridge; methyl terminal; structural properties; photoluminescence; elemental composition; spectroscopic ellipsometry

Preprints.org is a free multidiscipline platform providing preprint service that is dedicated to making early versions of research outputs permanently available and citable. Preprints posted at Preprints.org appear in Web of Science, Crossref, Google Scholar, Scilit, Europe PMC.

Copyright: This is an open access article distributed under the Creative Commons Attribution License which permits unrestricted use, distribution, and reproduction in any medium, provided the original work is properly cited.

Preprints (www.preprints.org) | NOT PEER-REVIEWED | Posted: 31 July 2023 doi:10.20944/preprints202307.2068.v1

Disclaimer/Publisher's Note: The statements, opinions, and data contained in all publications are solely those of the individual author(s) and contributor(s) and not of MDPI and/or the editor(s). MDPI and/or the editor(s) disclaim responsibility for any injury to people or property resulting from any ideas, methods, instructions, or products referred to in the content.

Article

Structural and Luminescence Properties of Eu-Doped PMO Films with Ethylene Bridge and Methyl Terminal Groups

Md Rasadujjaman [1,2,*], Jinming Zhang [1], Alexey S. Vishnevskiy [3], Jing Zhang [1,*] and Mikhail R. Baklanov [1,3,4]

[1] Department of Microelectronics, North China University of Technology, Beijing 100144, China; jinming@naura.com (J.Z.); baklanovmr@gmail.com (M.R.B.)
[2] Department of Physics, Mawlana Bhashani Science and Technology University, Santosh, Tangail 1902, Bangladesh; rasadphy@mbstu.ac.bd (M.R.)
[3] Research and Education Center "Technological Center", MIREA—Russian Technological University (RTU MIREA), Moscow 119454, Russia; alexeysw@mail.ru (A.S.V.)
[4] Research European Centre for Knowledge and Technology Transfer (EUROTEX), Brussels 1040, Belgium
* Correspondence: rasadphy@mbstu.ac.bd (M.R.); zhangj@ncut.edu.cn (J.Z.)

Abstract: Nanoporous films of Eu-doped organosilicate glass (OSG) have been synthesized using sol-gel technology and spin-coating, employing evaporation-induced self-assembly (EISA), on silicon wafers. The Eu doping is achieved by dissolution of $Eu(NO_3)_3 \cdot 6H_2O$ in the precursor solution. The deposited films are characterized by using Fourier transform infrared (FTIR) spectroscopy, ellipsometric porosimetry (EP), X-ray photoelectron spectroscopy (XPS) and photoluminescence spectroscopy. It is observed that Eu doping makes the films more hydrophilic and reduces the pore size and open porosity. The reduction $Eu^{3+} \rightarrow Eu^{2+}$ occurs in the pores of OSG films, which is confirmed by depth profiling XPS. However, Eu^{3+} still presents on the film's top surface. Presence of Eu^{3+} and Eu^{2+} gives characteristic luminescence emission in the range of 600–630 nm (Eu^{3+}) and 290–400 nm (Eu^{2+}). The Eu^{2+}/Eu^{3+} concentrations ratio depends on CH_3 groups concentration in the films. Moreover, concentration of Eu^{2+} ions in the pores can be reduced by exposure in inductively coupled (ICP) oxygen plasma. The observed shift of the luminescence spectra towards the UV region, in comparison to previously reported Eu-doped organosilicate films, can be attributed to the energy transfer occurring between the host material and Eu^{2+} ions.

Keywords: organosilica glass; europium; ethylene bridge; methyl terminal; structural properties; photoluminescence; elemental composition; spectroscopic ellipsometry

1. Introduction

Europium-doped materials are significant contenders for utilization in Si photonics, encompassing the production of light sources and optical amplifiers [1]. The advantage of Eu-doped materials stems from their ability to accommodate two distinct oxidation states (Eu^{3+} and Eu^{2+}), setting them apart from other commonly employed rare earth ions in photonics, such as Erbium (Er) or Ytterbium (Yb), which remain stable solely in the trivalent oxidation state [2–4]. A specific prerequisite involves the utilization of a Eu-containing host materials that are compatible with CMOS processing. The most straightforward approach that has been adopted entails incorporating Eu ions as dopants into a silicon oxide matrix [5,6].

However, the effectiveness of this approach is significantly hindered by the limited solubility of Eu in SiO_2 matrix, resulting in extensive clustering and precipitation phenomena [7,8]. Thus, the primary challenge for utilizing Eu in photonics lies in finding a host matrix that can be synthesized and processed in accordance with Si technology, while also being capable of accommodating high concentrations of optically active Eu ions and enabling control over the Eu oxidation state. Previous

© 2023 by the author(s). Distributed under a Creative Commons CC BY license.

Preprints (www.preprints.org) | NOT PEER-REVIEWED | Posted: 31 July 2023 doi:10.20944/preprints202307.2068.v1

research done by Bellocchi et al. [2,3,9] has demonstrated that a SiOC matrix (carbon-doped oxide) possesses favorable chemical properties, allowing for efficient promotion of the reduction of Eu^{3+} to Eu^{2+}, and structural properties that enhance the mobility and solubility of Eu ions, consequently minimizing Eu precipitation. Eu^{3+} and Eu^{2+} ions can function as highly effective emitting centers in the visible region. Eu^{2+} ions demonstrate a remarkably strong emission resulting from dipole-allowed $4f^65d \rightarrow 4f^7$ transitions. The intra 4f-shell transition of Eu^{3+} ions, being electric dipole-forbidden, results in a less intense luminescence [10,11]. It is well-established that the positions of emission bands of Eu^{2+} are highly dependent on the host materials'. In crystalline materials, the wavelength of photoluminescence (PL) emission is strongly influenced by the crystal field splitting of the 5d excited level. As the covalency between Eu^{2+} and ligands increases, the emission peak shifts towards longer wavelengths. For instance, in halide hosts, the shift occurs towards the near-violet to blue region due to the presence of highly electronegative halogen ions. However, in nitrides, the shift occurs at longer wavelengths due to the lower electronegativity of N^{3-} ions [12,13].

SiOC films have extensive use in CMOS technology as low dielectric constant (low-k) dielectrics for advanced interconnects. When combined with low resistivity metals (Cu, Co, Ru), they help reduce signal propagation delay in the interconnects of ULSI devices [14]. The majority of SiOC films employed in the microelectronics industry are deposited using PECVD (Plasma-Enhanced Chemical Vapor Deposition) processes and exhibit random porosity, with methyl groups making them hydrophobic [15]. The matrix structure of these films resembles that of SiO_2. However, currently, the interconnects developing community is increasingly focusing on periodic mesoporous organosilicates (PMOs). PMOs exhibit ordered porosity and may use a wide variety of carbon bridges within their matrix [16–18]. The major advantage of these materials is improved mechanical properties that potentially increases the reliability of integrated devices [15,19,20]. Hence, Eu-doped PMO films exhibit considerable potential as parts of nanophotonic devices and optical interconnects suitable for integration into the back end of the line (BEOL) structures within Ultra-Large-Scale Integration (ULSI) systems.

It is important to note that various bulk PMO materials with diverse organic bridges have already been investigated as potential hosts for Eu and other rare-earth (RE) metals. The significant findings have been examined and consolidated in the review paper [21]. However, the distinctive characteristic of our materials lies in their thin film nature and the simultaneous presence of carbon bridges and methyl terminal groups.

Hence, our focus has been on investigating the potential of periodic mesoporous organosilicate (PMO) films as host materials for rare-earth metals. Our aim is to analyze the chemical and structural modifications of PMO films upon the incorporation of metal (Eu) ions and to compare the luminescent properties of these materials with those of previously reported SiCOH and SiO_2 films. Specifically, the objective of this study is to examine thin porous PMO films containing both ethylene bridges and methyl terminal groups, incorporating Eu ions.

2. Materials and Methods

2.1. Materials

PMO films were synthesized using the sol-gel method by spin-on deposition on silicon wafers. The method involves acid-catalyzed hydrolysis and polycondensation processes [16]. The carbon sources used were 1,2-bis(trimethoxysilyl)ethane (BTMSE, 96%, Sigma-Aldrich) monomer (as the source of ethylene groups) and methyltrimethoxysilane (MTMS, 98%, Fluka) monomer (as the source of terminal methyl groups). These precursors ensure the presence of ≡Si–$(CH_2)_2$–Si≡ and ≡Si–CH_3 groups, respectively, in the resulting polymers, as the ethylene and terminal methyl groups do not undergo hydrolysis. A surfactant (porogen) called Brij30 ($C_{12}H_{25}(OCH_2OCH_2)_4OH$ with a molecular weight of 362 g/mol, Sigma-Aldrich) was used to facilitate the evaporation induced self-assembly (EISA [22]) process and obtain a porous structure. The molar ratio of BTMSE/MTMS/deionized water was 0.47/0.53/3.087, and a little amount of a 0.0053 M HCl was added as a catalyst. The prepared solution was stirred and aged for ~12 hours at 60°C and then stored for 24 hours at room temperature

Preprints (www.preprints.org) | NOT PEER-REVIEWED | Posted: 31 July 2023 doi:10.20944/preprints202307.2068.v1

(RT) before spin coating of PMO films. The matrix solution was divided into four, and the different weight percent (wt%) of Brij30 surfactant (0, 10, 20 and 30 wt%) was added into four solutions and stirred. Those films were labeled as pristine PMO films. Then, the different amount (0.0, 1.7, 12.1 and 25.8 wt%) of $Eu(NO_3)_3{\cdot}6H_2O$ precursor powder were added into the four stored solution for spin coating of Eu-doped PMO films, respectively. The appropriate proportion of ethanol as solvent was also used before coating the films. The final coating solution was used to deposit films on 150 mm diameter silicon wafers (1–10 Ω.cm) with a spin coater at an acceleration rate of 500 rpm for 5 sec and a spinning rate of 4500 rpm for 30 seconds. After deposition, the films were cured on the hot plate at 150 °C for 40 min in air (soft bake (SB) to remove solvents), and the final curing was done at 400°C, 20 min in air (hard bake (HB)) to remove template (porogen) and produce the final porous films.

2.2. Characterization Methods

2.2.1. Fourier-transform infrared (FTIR) spectroscopy

Fourier-transform infrared (FTIR) spectroscopy. FTIR spectra were recorded to study the chemical composition of the films. The spectra were obtained by using FTIR, JASCO FT/IR-6300, scanned 64 times in transmission mode with a resolution of 4 cm^{-1} and a measurement wavenumber range of 4000–400 cm^{-1}. The wavenumber accuracy and maximum resolution were within ±0.01 cm^{-1} and 0.07 cm^{-1}, respectively. The high-intensity ceramic source light source, gold 28° Michelson interferometer with auto-alignment mechanism and a Ge/KBr beam splitter with signal to-noise ratio of 50000:1 was used for the measurements. The background spectra were obtained by using a pure silicon (1–10 Ω·cm) sample cut from the same wafer that was used for the film deposition. After background subtraction all the spectra were normalized to the highest Si–O–Si peak.

2.2.2. Ellipsometric Porosimetry (EP)

In this work, the EP system uses a SENpro spectroscopic ellipsometer with SpectraRay/4 software for the data analysis (SENTECH, Germany) with λ = 350–850 nm. Atmospheric pressure ellipsometric porosimetry was used to evaluate the porosity and pore size distribution [23,24]. The angle of light incidence was fixed at 70°. Heptane vapor diluted by N_2 carrier gas was used as an adsorptive. The films open porosities were calculated as the volume of condensed liquid adsorptive (V) from RI values measured during the heptane adsorption by using the Lorentz–Lorenz equation [21]. The calculation of the pore size of the mesoporous film is based on the Kelvin equation. The size of the micropores is calculated by using the Dubinin–Radushkevich equation adapted for EP [21].

2.2.3. X-ray Photoelectron Spectroscopy (XPS)

XPS analysis was performed using a PHI 5300 (PerkinElmer, Fremont, CA, USA) to investigate the point (500 μm) depth profile of OSG films under UHV conditions at a base pressure of 5×10^{-8} torr during the operation. The samples were transported in an inert gas environment prior to the insertion into the XPS machine, and exposure to air was reduced to a minimum. The experiments were performed with a monochromated Al Kα radiation source (E= 1.487 keV). Photoelectron detection was conducted with a constant analyzer energy (CAE) analyzer and a 2D delay-line detector and with a standard lens mode. An electron flood gun was utilized during measurements to compensate for surface charging. Individual component (C, O, Eu, Si) peaks and survey scan were measured at a pass energy of 20 eV and 100 eV, respectively. Survey scans were conducted in the 0–1100 eV range. The peaks were fitted using the Origin 2019b software by Gaussian functions.

2.2.4. Photoluminescence Spectroscopy (PL)

The UV induced luminescence spectra of pristine and Eu-doped nanoporous PMO films were measured by JASCO FP-8300 spectrofluorometer by using a continuous output Xe arc lamp with shielded lamp housing (150 W) and holographic concave grating in modified Rowland mount monochromator. The Radio-photometer system using monochromatic light was used to monitor the

Preprints (www.preprints.org) | NOT PEER-REVIEWED | Posted: 31 July 2023 doi:10.20944/preprints202307.2068.v1

intensity output of the Xe lamp. The samples were mounted in a standard cell holder (10 mm rectangular cell holder) SCE-846/D061161450 provided by JASCO. The wavelength accuracy and maximum resolution is 1 nm. The excitation was used from 200 nm (6.2 eV) under room temperature the emission spectra range in wavelength from 210 nm to 500 nm and slit width is 5nm–5nm. The measurements were fully controlled by using a Spectra Manager. The excitation and emission bandwidth were 5 nm with scan speed 1000 nm/min.

3. Results

3.1. Chemical composition (FTIR data)

Chemical composition (FTIR data). The FTIR spectra of fully cured nanoporous (porosity-25%, pore size-1.04 nm) Eu-doped (0–25.8 wt%) OSG films are shown in Figures 1 and 2. The absorption bands at 3700–3000, 3000–2950, 1300–1000 cm^{-1} correspond to hydroxyl and silanol groups (O–H and Si–OH), methyl group (–CH_3) and Si–O–Si stretching modes, respectively [25]. The pristine films (0 wt% Eu) almost does not show the presence of Si–OH and adsorbed water at 3700–3000 cm^{-1} (Figures 1 and 2a). The increase in the Eu concentration decreases the concentration of –CH_3 group (3000–2950 cm^{-1}) and Si–CH_3 groups (1250–1270 cm^{-1}) (Figures 1 and 2b,c). As could be expected, the films become more hydrophilic. The reduction in the concentration of CH_3 (and Si–CH_3) groups primarily occurs in the films deposited with 1.7 wt% of $Eu(NO_3)_3{\cdot}6H_2O$. Further increases in Eu concentration show insignificant effects. It is observed that the highest hydrophilicity corresponds to a moderate Eu concentration of 12.1%. Conversely, the film doped with 25.8 wt% of $Eu(NO_3)_3{\cdot}6H_2O$ is more hydrophobic than both the 1.7 wt% and 12.1 wt% Eu-doped films. Additionally, there are less pronounced features, including an increase in the concentration of CH_2 groups in the sample doped with 25.8 wt% of $Eu(NO_3)_3{\cdot}6H_2O$ (Figure 2b, region 2850–2930 cm^{-1}, which normally reflects the presence of hydrocarbon residues formed during porogen removal [26]), and a slight red shift of the Si–O–Si peak (Figure 2c).

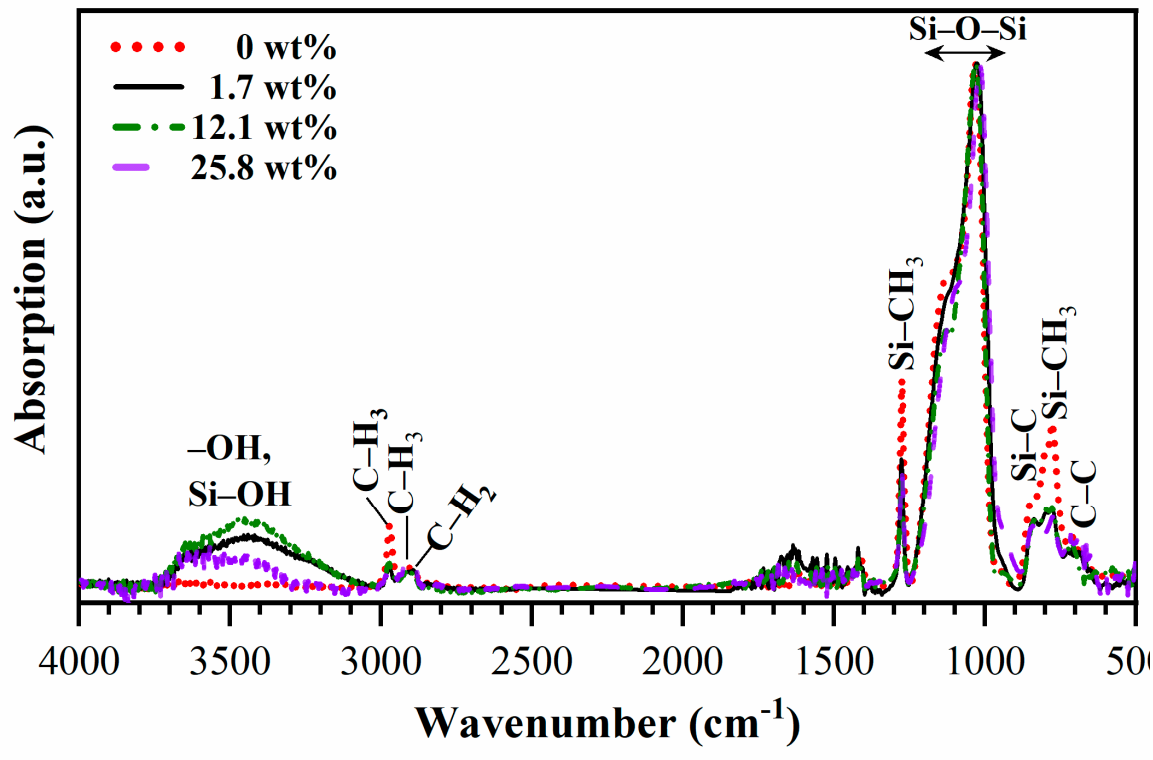

Figure 1. FTIR survey spectra of Eu-doped PMO films deposited with a BTMSE/MTMS precursors ratio of 47/53 and porogen concentrations 20 wt% after hard bake (HB) at 400 °C for 30 min in the air.

Preprints (www.preprints.org) | NOT PEER-REVIEWED | Posted: 31 July 2023 doi:10.20944/preprints202307.2068.v1

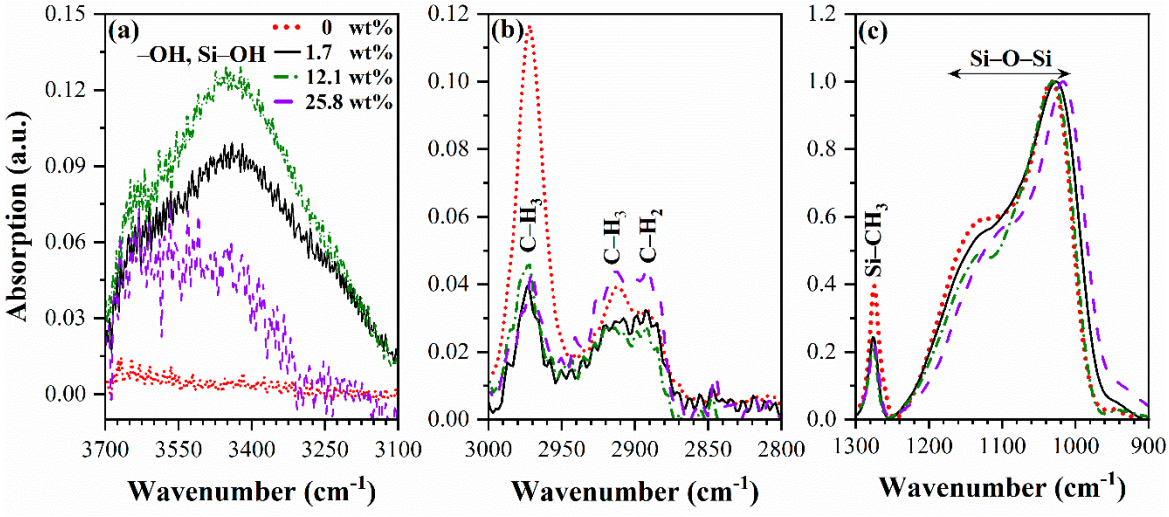

Figure 2. Zoom of FTIR spectra in the regions: (a) to Si–OH/water (3100–3700 cm^{-1}), (b) CH_x groups (2800–3000 cm^{-1}), (c) Si–O–Si (900–1200 cm^{-1}) and $Si–CH_3$ (1240–1300 cm^{-1}).

3.2. Porosity and pore size distribution

Porosity and pore size distribution. Figure 3 shows adsorption–desorption isotherms of heptane vapors measured by EP and calculated pore size distribution of different Eu-doped nanoporous OSG films. The films with the 0 wt% Eu concentration shows isotherms without a hysteresis loop. However, Eu introduction reduces open porosity from 25% (pristine, non-doped film) to 14% (25.8 wt.%) (Figure 3 a,d). The corresponding change of refractive index (RI) during adsorption, 1.33–1.43 (0 wt%); 1.32–1.43 (1.7 wt%); 1.32–1.4 (12.1 wt%); 1.34–1.41 (25.8 wt%), show that initial RI value reflecting the full porosity [21,22] is not changing. If to assume that skeleton (matrix) of non-doped film has RI close to 1.46 (dense SiO_2), we can calculate that the full porosity is equal to 25.5%, which is very close to the open porosity of un-doped films (Table 1). Therefore, it is reasonable to assume that reduction of open porosity is related to "blocking" of some open pores against the heptane adsorption (Figure 4) while the change of the full porosity is small. Furthermore, the isotherms observed for samples 3 and 4 exhibit characteristic signs typical of narrow slit-shaped pores (type H4 isotherm in Refs. [27,28], Figure 3c,d, P/Po > 0.2). Specifically, the presence of narrow slit-shaped pores indicates an initial stage of pore blocking. Reduction of pore size and internal surface area of bulk (not thin films) PMO materials after grafting by Rare Earth (RE) metals has already been observed and reported in the papers [29,30]. The pore blocking effect increases with Eu concentration and probably can also explain reduction of air adsorbed moisture amount when Eu precursor concentration increased from 1.7 to 25.8 wt%.

Table 1. The most important characteristics of PMO films used in these experiments.

Sample Number	$Eu(NO_3)_3·6H_2O$ Content, wt%	Thickness, nm	RI	Full Porosity, %	Open Porosity, %	Pore Diameter, nm
1	0	478.0	1.325	26.5±1	23.7±1	1.8±0.1
2	1.7	493.6	1.329	25.7±1	24.3±1	1.9±0.1
3	12.1	485.2	1.333	25.9±1	20.7±2	1.8±0.1
4	25.8	465.7	1.320	27.6±1	13.5±2	1.8±0.1

Preprints (www.preprints.org) | NOT PEER-REVIEWED | Posted: 31 July 2023 doi:10.20944/preprints202307.2068.v1

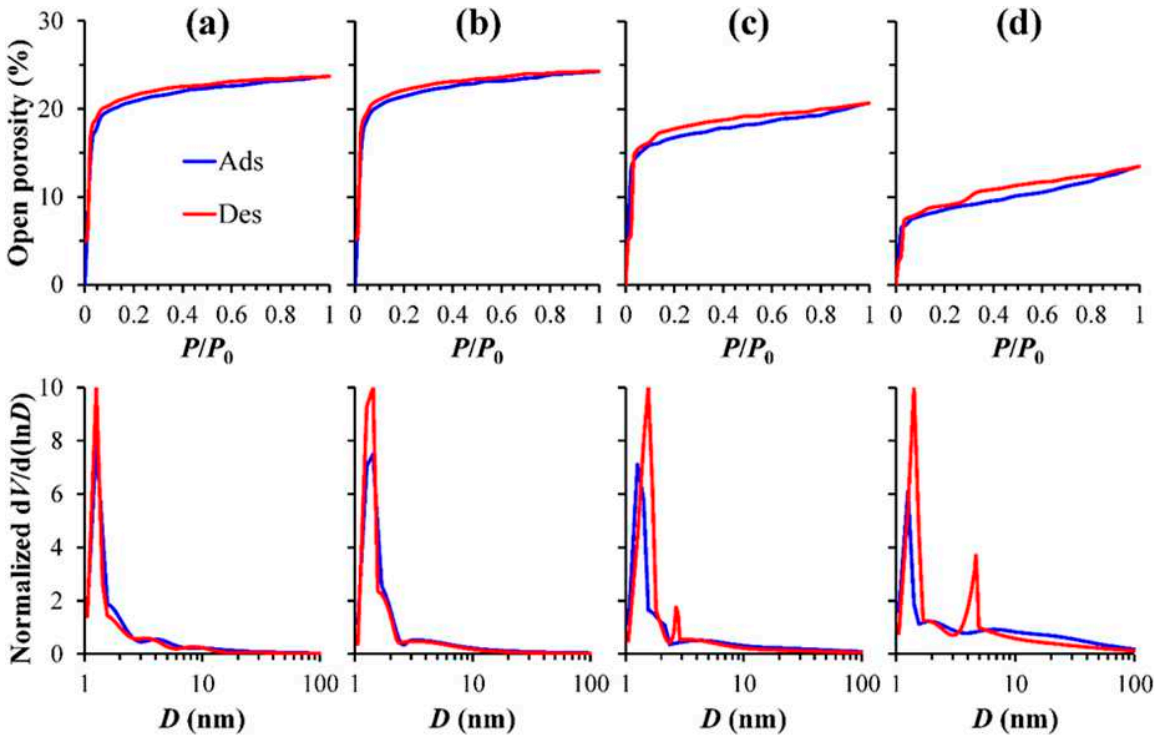

Figure 3. Adsorption–desorption isotherms and pore size distribution of (a) 0 wt% (b) 1.7 wt% (c) 12.1 wt% and (d) 25.8 wt% Eu-doped in the 25% porosity (20 wt% Brij30) OSG films.

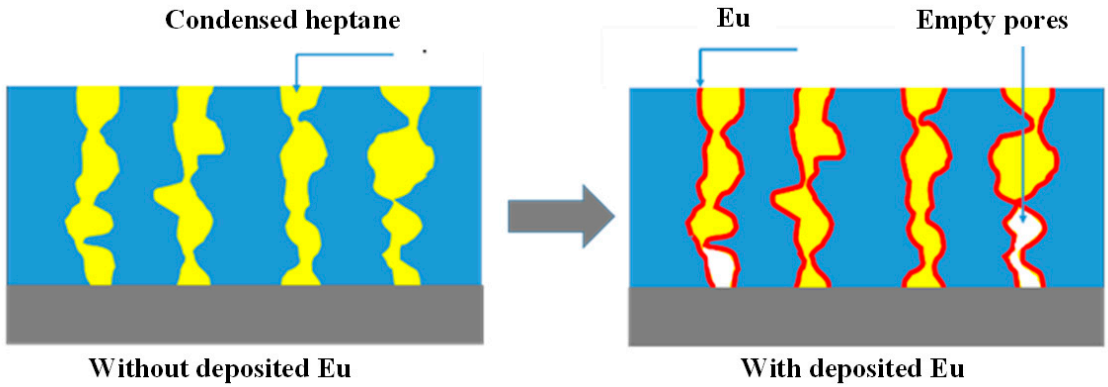

Figure 4. In the pristine film (left), the full porosity is equal to the open porosity (Table 1) because all the pores are interconnected for heptane adsorption. However, after Eu deposition, some parts of pores become inaccessible to heptane adsorption (parts of 1 and 4 pores). It reduces the measured open porosity while the full porosity remains the same as in the pristine film.

3.3. X-ray Photoelectron Spectroscopy Analysis (XPS)

The XPS measurements were done only for the 25.8 wt% Eu doped PMO films deposited with BTMSE/MTMS ratio equal to 47/53 and open porosity 13% (Table 1). It is shown that the deposited films are mainly composed by C, O, Si, and Eu (Figure 5). Figure 5a clearly illustrates the presence of Eu^{3+} on the film top surface (not etched sample) [31]. However, Eu^{3+} almost completely disappears after a 62-second ion beam etching process, and only Eu^{2+} is observed thereafter, even for longer durations. Furthermore, compared to the sample etched for 62 seconds, the low-k surface exhibited an enrichment of oxygen, carbon, and silicon (Figure 5b,c,d). To analyze the depth profile of components, the low-k films were etched using a focused ion beam with a rate of approximately 17 nm/min. Eu^{3+}/Eu^{2+} ratio during the etching drastically decreases already after 61 seconds etch that corresponds to 17 nm. Further etching is almost not changing this ratio (Figures 5 and 6). These data

Preprints (www.preprints.org) | NOT PEER-REVIEWED | Posted: 31 July 2023 doi:10.20944/preprints202307.2068.v1

confirm that Eu^{3+} presents only on the film surface while only Eu^{2+} presents in the film bulk. Some differences between surface and bulk can also be seen in oxygen XPS spectra (Figure 5b). The film surface is characterized by presence of O 1*s* peak located below 530 eV but this peak disappears after ion beam etch and O 1*s* only represented by the peak with energy about 532 eV. The first peak is most probably related to surface contamination by carbon as it was suggested in Ref. [32]. The peaks position of Si 2*P* and C 1*s* is typical for organosilicate based low-k materials [33] and do not change during the depth profiling. However, the film surface also exhibits enrichment of these components, which could indicate surface contamination. (Figure 5c,d).

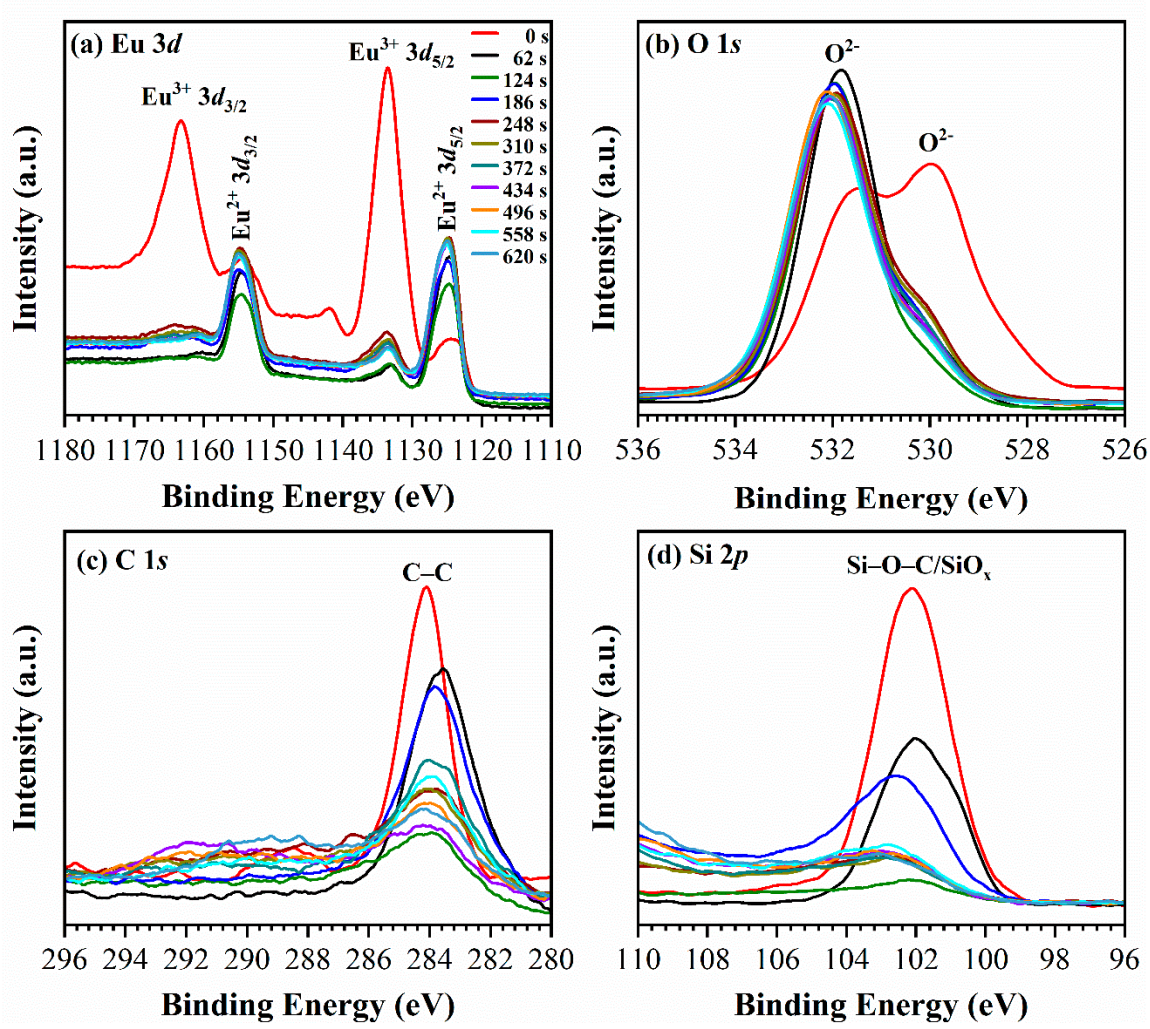

Figure 5. The XPS spectra showing the comparison between the 25.8 wt% Eu-doped nanoporous OSG film (20 wt% Brij30 sample) deposited on a Si substrate (red curve) and the film after undergoing stepped ion beam etching for a duration ranging from 62 to 620 seconds.

The distribution of Eu within the low-k film is highly uniform, with a concentration of approximately 10 atomic percent (at%). The surface region exhibits a higher concentration of Eu, approximately 17 at%. The dopant concentration was determined based on the weight percentage (wt %) of $Eu(NO_3)_3{\cdot}6H_2O$ in the precursor mixture. Estimations of the Eu ion concentration in the film components from the precursors indicate that 25.8 wt% of $Eu(NO_3)_3{\cdot}6H_2O$ corresponds to 10 at% of Eu ions in the films. For detailed calculations and estimations, please refer to the Supplementary Materials.

Preprints (www.preprints.org) | NOT PEER-REVIEWED | Posted: 31 July 2023 doi:10.20944/preprints202307.2068.v1

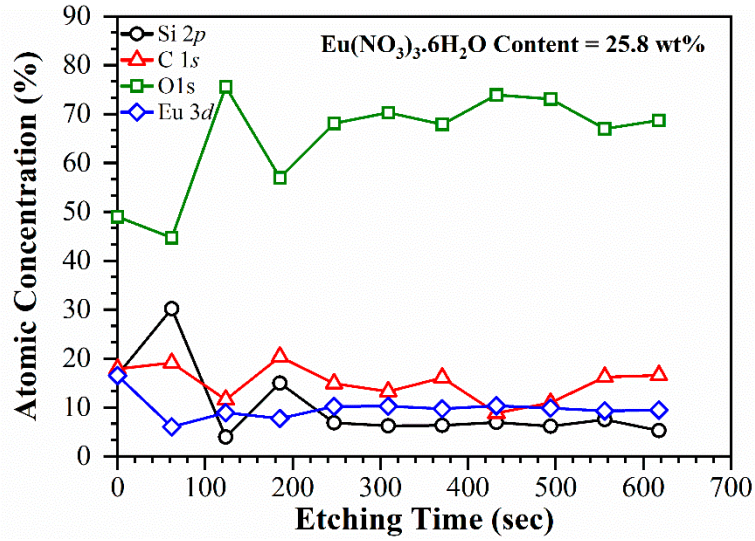

Figure 6. The atomic concentration profile of the components in the 25.8 wt% Eu-doped nanoporous OSG films plotted as a function of ion-beam etching time.

3.4. UV-induced luminescence

The photoluminescence spectra of 0 wt% Eu (pristine) and 12.1 wt% Eu-doped soft bake (SB) and hard bake (HB) nanoporous OSG films are shown in Figure 7. Pristine sample (fully cured) shows single PL peak located near 300 nm (4.2 eV), which is related to presence of methyl terminal group and carbon residue [34]. Thermal curing enhances the intensity of photoluminescence and broadens the emission spectra. Furthermore, in the PL region, the peaks display a duplicated structure, characterized by distinct peaks around 290 nm and 314 and 348 nm (Figure 7b). The peak at 290 nm coincides with the matrix luminescence. One notable characteristic is that in all previous publications discussing luminescence from SiO_2 and SiCOH materials doped with Eu^{2+}, the PL peaks were consistently found at longer wavelengths, typically within the range of 400–500 nm. Additionally, it is clear that thermal annealing enhances the PL intensity and triggers PL emissions within the 580–720 nm range. This effect is directly influenced by the annealing temperature, with the highest intensity observed after a rigorous bake at 400 °C.

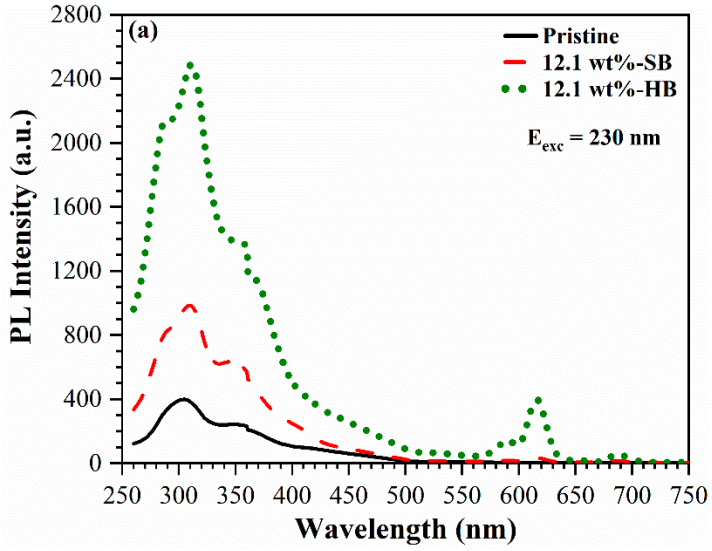

Preprints (www.preprints.org) | NOT PEER-REVIEWED | Posted: 31 July 2023 doi:10.20944/preprints202307.2068.v1

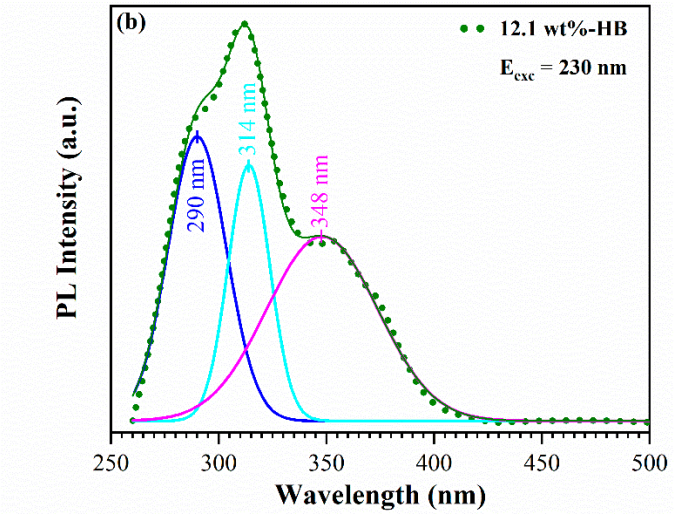

Figure 7. (a) Photoluminescence spectra of 0 wt% Eu (pristine), 12.1 wt% Eu-doped soft bake (SB) and 12.1 wt% hard bake (HB) OSG films. (b) deconvolution of the broad peak in the 250–500 nm region. Deconvolution of 580–720 nm PL will be presented later in the section related to a more detailed analysis of the photoluminescence in this region.

The peaks located in the region 580–720 nm are well known and they are related to emission of Eu^{3+} ions (Figure 7) and electronic transitions $^5D_0$–$^7F_1$ (589 nm), $^5D_0$–$^7F_2$ (615 nm) and $^5D_0$–$^7F_4$ (689 nm) [35–38]. SB samples show much less intensive photoluminescence in comparison with HB samples. The primary explanation is associated with the presence of residual solvent impurities and adsorbed moisture in the SB samples. Numerous reports have highlighted the significance of internal quenching through hydroxide (OH–) impurities and surface quenching via surface hydroxyl groups [39,40].

The PL quenching mechanism involves energy transfer from excited Eu atoms to the surface hydroxyl groups incorporated due to water adsorption. Importance of PL quenching related to presence of moisture impurities can also be clearly seen in temperature dependence (Figure 8). The maximum PL intensity is observed in the sample annealed at 400°C. It is known from microelectronic experience that this temperature is sufficient for removing porogen and adsorbed moisture, which is why it is used as the final curing temperature for low-k films [41,42]. However, contrary to other Eu-doped silica and PMO materials, further increasing the temperature reduces the PL intensity of our material. The reason for this is that our material also contains methyl terminal groups that have limited temperature stability, particularly close to 500°C.

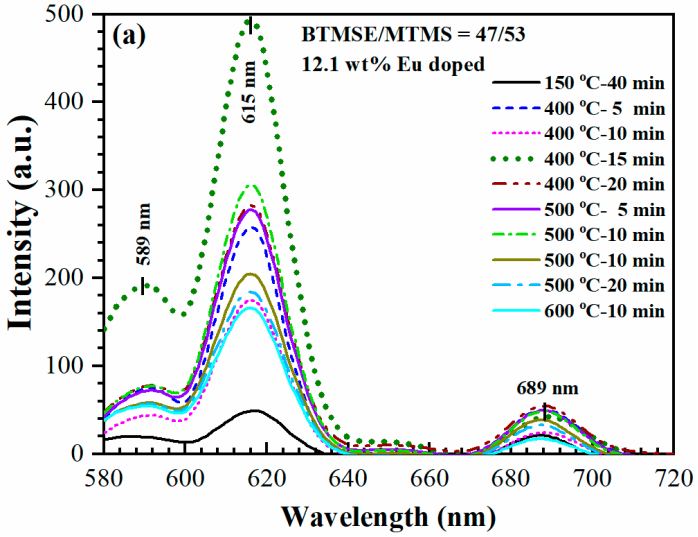

Preprints (www.preprints.org) | NOT PEER-REVIEWED | Posted: 31 July 2023 doi:10.20944/preprints202307.2068.v1

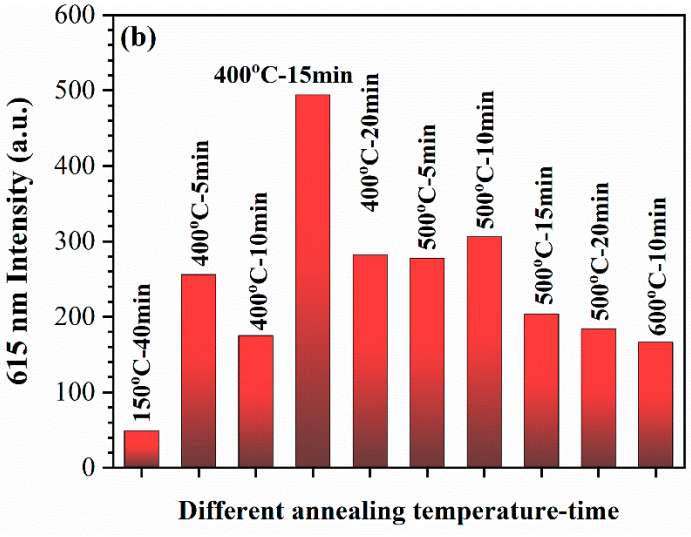

Figure 8. Dependence of PL intensity on annealing temperature.

Figure 9 also shows that the PL intensity in this region depends on Eu concentration. First it increases with Eu concentration 0–12.1 wt%, then drops at 25.8 wt%. It is known that a high concentration of Eu doping reduces the distance between Eu ions, stimulating the non-radiative relaxation process and leading to cross relaxation between neighbouring Eu ions, which results in a decrease in luminescence efficiency [43,44]. Practical fluorescence quenching, caused by the aggregation of Eu^{3+}, becomes evident in silica glass when the Eu content exceeds 1% (molar ratio) [45]. In our study, fluorescence quenching occurs at a higher Eu concentration due to the significantly larger internal surface area of mesoporous organosilicate films. Figure 10 demonstrates the dependence of photoluminescence intensity on the wavelength of the excited light. The highest PL intensity is observed when the excitation wavelength is 230 nm, which aligns with previously reported data [34].

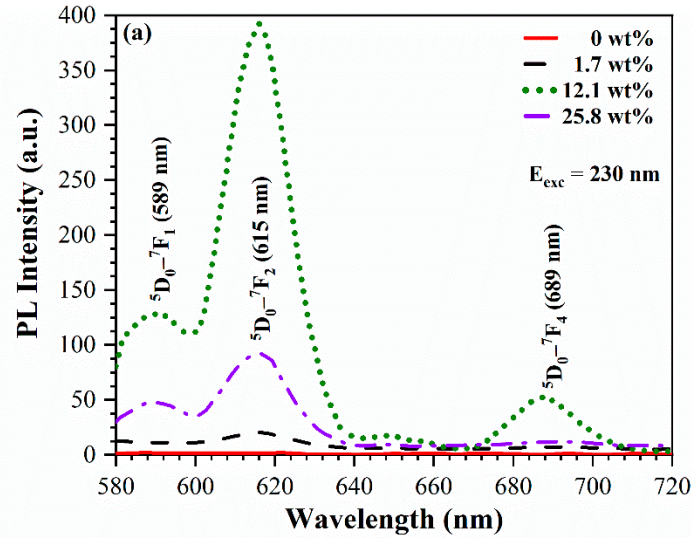

Preprints (www.preprints.org) | NOT PEER-REVIEWED | Posted: 31 July 2023 doi:10.20944/preprints202307.2068.v1

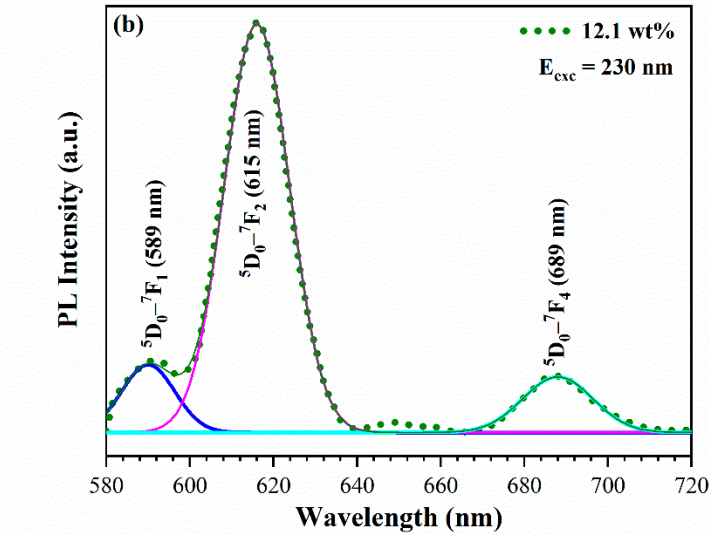

Figure 9. (a) Eu^{3+} photoluminescence intensity versus $Eu(NO_3)_3{\cdot}6H_2O$ concentration in the precursor Sol (wt%) upon excitation with light of 230 nm. (b) deconvolution of the PL spectra of the sample deposited with 12.1 wt% of $Eu(NO_3)_3{\cdot}6H_2O$ to peaks corresponding to well-known ^5D–^7F transitions in Eu^{3+}. Dependence of PL intensity on annealing temperature.

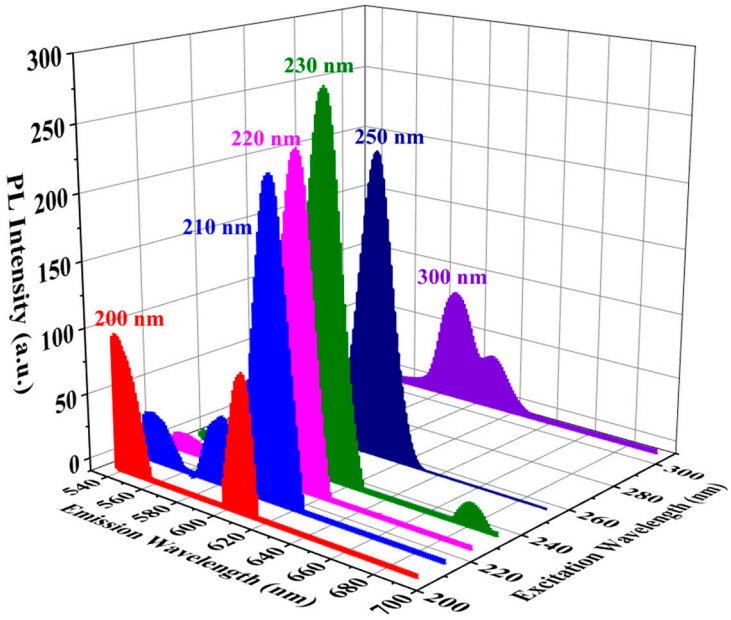

Figure 10. Dependence of PL intensity on wavelength of excited UV light. The maximum PL intensity is observed at 230 nm excitation wavelength.

3.4.1. Effect of oxygen plasma

Figure 11 shows effect of exposure to inductively coupled (ICP) oxygen plasma [46] The red curve shows PL spectra of Eu doped sample that was stored in air several days after deposition. Spectra clearly show PL from Eu^{3+} (550–700 nm) and Eu^{2+} (250–500 nm). PL emission from Eu^{2+} has well pronounced peaks near 300 and 350 nm and is more than an order of magnitude intense than the PL from Eu^{3+}. Exposure to oxygen plasma results in a reduction of PL emission from Eu^{2+} and an increase in PL from Eu^{3+} (Figure 11). This observation strongly suggests that the Eu^{2+} ions formed during the process undergo oxidation by the oxygen plasma. However, the depth of penetration of oxygen radicals from the plasma into the pores of low-k materials is limited and influenced by various factors, including radical concentration, pore size, and the chemical groups that are

Preprints (www.preprints.org) | NOT PEER-REVIEWED | Posted: 31 July 2023 doi:10.20944/preprints202307.2068.v1

consuming the radicals [47]. In the case of pristine low-k films, the consumption of oxygen radicals is primarily associated with terminal CH_3 groups. However, in the present scenario, the oxygen radicals is also consumed in the oxidation of Eu^{2+} ions. The decrease in photoluminescence intensity in the 330–250 nm range suggests that the fraction of oxidized Eu^{2+} ions does not exceed 50%, indicating that the depth of modification was approximately 250 nm (the total film thickness is about 500 nm).

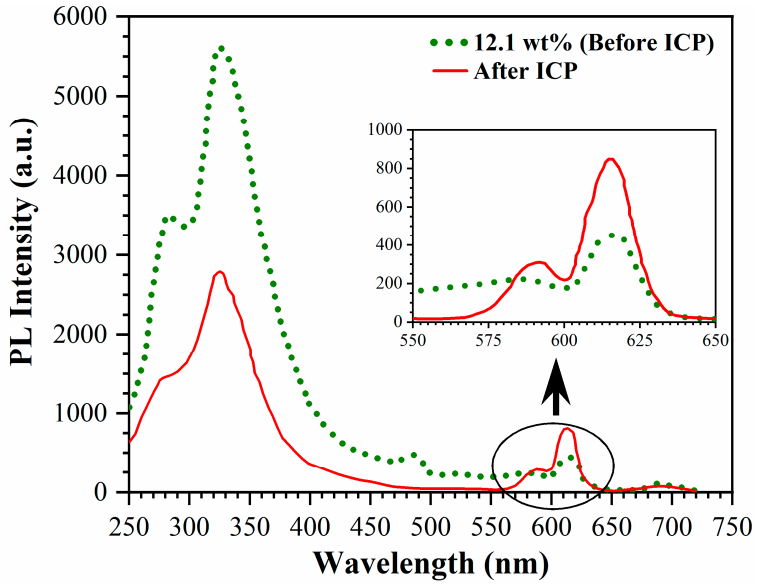

Figure 11. Effect of ICP oxygen plasma on PL intensity of Eu^{3+} and Eu^{2+} upon excitation with light of 230 nm. Inset shows the zoom PL spectra of 550–650 nm region.

4. Discussion

The XPS results clearly demonstrate that Eu^{3+} ions are exclusively present on the top surface of PMO films, while only Eu^{2+} is observed within the pores. The coexistence of Eu^{3+} and Eu^{2+} significantly enhances the total photoluminescence (PL) intensity and even extends the spectral range into the ultraviolet (UV) region. It is worth noting that Eu in our case was introduced into the film's precursor in its 3-valent state as $Eu(NO_3)_3{\cdot}6H_2O$, and it is making the mechanism of Eu^{3+} reduction inside the pores intriguing. However, the reduction of Eu^{3+} in porous materials (or in matrix of dense materials) has been extensively reported in the literature. Numerous mechanisms have been proposed in different papers (see, for instance, Refs. [41,48,49] and others. The most popular explanation of Eu^{3+} reduction to Eu^{2+} in silica-based materials being the impact of ejected electrons from oxygen-associated hole centers. Zaitoun et al. [50,51] studied luminescence properties of Eu^{3+} encapsulated in sol-gel-derived optically transparent silica gels using time-resolved laser spectroscopy. It was proposed that the electron-hole carriers, e^-–h^+, were generated during the polycondensation reaction of silica and trapped at the defect sites of sol-gel matrix. The formation of e^-–h^+ carrier was proposed to be responsible for the surface-assisted reduction of Eu^{3+} ions, where the ejected electrons from the oxygen-associated hole centers react with Eu^{3+} to produce Eu^{2+} ions. Later this mechanism was extended to other materials [52]. Numerous papers explain Eu^{3+} reduction by interaction with certain types of reduction groups present in the matrix. Eu^{3+} reduction to Eu^{2+} was observed in silica based films co-doped with Al^{3+} and B^{3+} and other metals when the films were annealed in reducing atmosphere at $T > 400°C$ [53–56]. Eu^{3+} reduction by carbon containing groups present in SiCOH films was proposed in works Boninelli et al. [2,3,9]. The last mechanism might be the most suitable for our PMO material because it contained similar carbon groups, as in the case of SiCOH films.

The host materials employed in this study were deposited as PMO films with well-defined porosity. These films contained ethylene bridges within their matrix and methyl terminal groups, which primarily localized on the pore wall after thermal curing (Figure 12) [57,58]. This characteristic

Preprints (www.preprints.org) | NOT PEER-REVIEWED | Posted: 31 July 2023 doi:10.20944/preprints202307.2068.v1

sets of PMO films apart from SiCOH films deposited through sputtering of SiO_2 and SiC targets [3,9] as well as via PECVD [13,37,53]. To introduce Eu doping into the PMO films, the film precursor was mixed with $Eu(NO_3)_3 \cdot 6H_2O$. Consequently, Eu ions are expected to be randomly distributed throughout the matrix in the as-deposited films. Additionally, Eu doping resulted in a decrease in the concentration of CH_3 groups. Similar to previous publications [2,3,9], it can be inferred that methyl groups play a critical role in reducing Eu^{3+} to Eu^{2+}. Two additional noteworthy observations for further analysis are the reduction in pore size (Figure 3) and an increase in the concentration of CH_2 groups (Figure 2b). Based on these findings, it is reasonable to propose that, akin to CH_3 groups, Eu ions also segregate onto the pore wall and establish chemical bonds with two CH_2 groups, resembling lanthanide carbides, reduces the pore size. Another possibility is formation of Eu silicate similar to Ref. [59]. However, in both cases one can expect the observed read shift in –Si–O–Si– peak (Figure 2c) because the groups replacing CH_3 are even more electropositive.

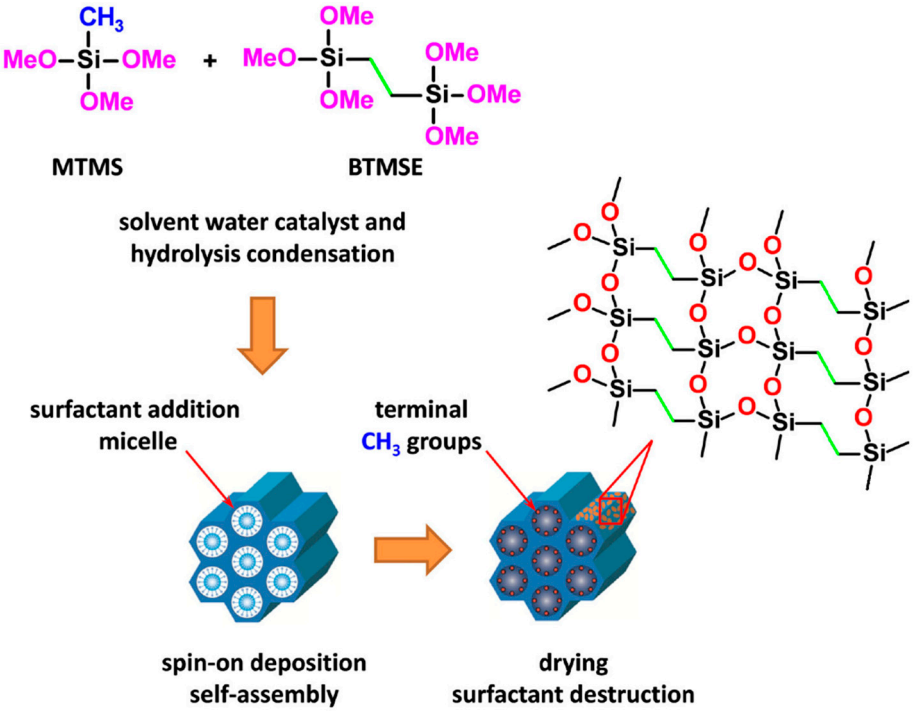

Figure 12. Schematic presentation of PMO material with ethylene bridging and methyl terminal groups fabricated with co-polymerization of MTMS and BTMSE and EISA deposition technology.

Several conclusions can be derived from the data pertaining to the exposure to oxygen plasma. It can be deduced that oxygen radicals exclusively oxidize Eu^{2+} ions located on the surface of the pores. This limitation arises due to the radicals' inability to diffuse into the film matrix without undergoing recombination. Conversely, the emission spectrum remains unaltered following exposure to oxygen plasma (see Figure 11). This observation implies that the positioning of Eu^{2+} ions within the film is accurately defined, indicating a narrow distribution of ion sites. Consequently, these findings supports our hypothesis that the Eu^{2+} ions were located on the surface of the pore walls.

To confirm the important role of methyl groups in formation of Eu^{2+} ions, experiments with different concentration of methyl groups were carried out. All the experiments discussed so far were conducted with PMO films deposited with a BTMSE/MTMS ratio 47/53. However, one special experiment was done with a film deposited with a BTMSE/MTMS ratio of 27/75. This MTMS-rich mixture was expected to produce a film with a much higher concentration of methyl groups. The results of the photoluminescence (PL) study on these samples are presented in Figure 13.

Preprints (www.preprints.org) | NOT PEER-REVIEWED | Posted: 31 July 2023 doi:10.20944/preprints202307.2068.v1

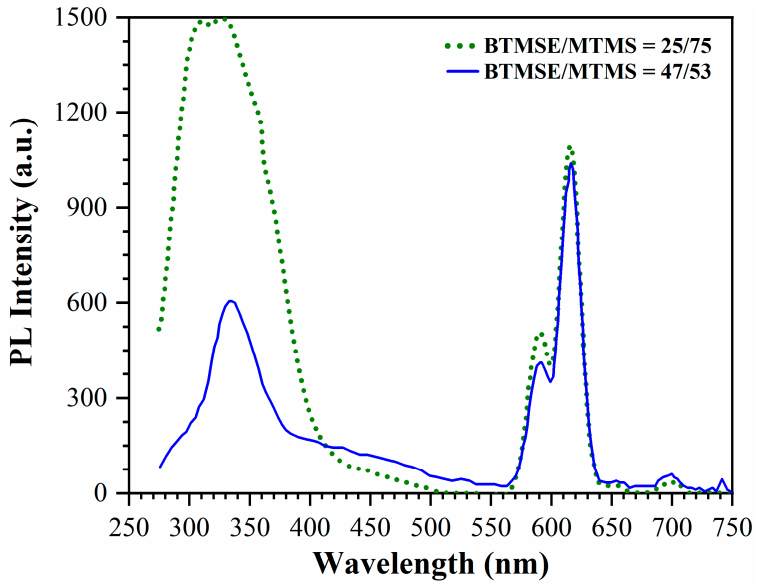

Figure 13. PL spectra of PMO films deposited with BTMSE/MTMS ratio 47/53 (solid line) and 25/75 (dotted line) upon excitation with light of 230 nm.

The first important observation is that the intensity of the peaks related to Eu^{3+} is the same in both cases. This is expected because the concentration of Eu^{3+} depends solely on the concentration of $Eu(NO_3)_3 \cdot 6H_2O$ introduced into the precursor solution and is independent of the BTMSE/MTMS ratio. Therefore, the amount of Eu^{3+} deposited on the top surface should be the same, as observed in Figure 13. However, the situation is different for the broad peak in the 275–400 nm region. The intensity of this peak is much higher in the film deposited with a BTMSE/MTMS ratio of 25/75. This indicates that the concentration of Eu^{2+}, which is likely responsible for this emission, increases with the concentration of CH_3 groups. It is worth mentioning that Eu^{2+} aqueous solution in air is known to be unstable, as it can be completely oxidized within 24 hours to form Eu^{3+} [38,60]. Therefore, Eu^{2+} is not formed in the precursor solution but rather in the already formed film. It forms relatively stable molecules that can only be oxidized by oxygen radicals generated in the ICP oxygen plasma.

The final question pertains to the position of the broad peak associated with the formation of Eu^{2+}. It has been suggested that the emission of Eu^{2+} in different compounds can vary from UV to blue wavelengths [11,61]. Most silica-based compounds containing Eu^{2+}, such as xerogel, SiCOH and PMO, exhibit photoluminescence in the blue light range with maximum located near 450 nm. However, in our case, the photoluminescence is shifted towards lower wavelengths.

Based on our findings, we can hypothesize the presence of an energy transfer mechanism whereby the highly efficient absorption properties of our PMO film in the short wavelength range are utilized to transfer excitation energy to the Eu^{2+} ions. This energy transfer mechanism enhances the photoluminescence (PL) efficiency of the Eu^{2+} ions when excited at shorter wavelengths. This hypothesis is further supported by the observation in Figure 7b, where one of the three deconvoluted peaks is located at the same wavelength as the host material but exhibits higher efficiency than the pristine material. Consequently, this energy transfer mechanism results in an overall increase in the PL efficiency of both the Eu^{2+} ions and the PMO matrix.

5. Conclusions

Nanoporous Eu-doped organosilicate glass films were synthesized using sol-gel technology and EISA-based deposition on Si wafers. EISA approach has allowed to achieve the pore ordering and these materials are termed as periodic mesoporous organosilicates (PMO) [17]. The Eu doping was achieved by dissolving $Eu(NO_3)_3 \cdot 6H_2O$ in precursor solutions based on BTMSE/MTMS mixtures, enabling the formation of both ethylene bridges in the film matrix and methyl terminal groups on the pore walls. The presence of both carbon bridges and methyl terminal groups is a standard

Preprints (www.preprints.org) | NOT PEER-REVIEWED | Posted: 31 July 2023 doi:10.20944/preprints202307.2068.v1

requirement in microelectronic technology for improved mechanical properties and hydrophobicity [14,16,30]. The deposited films were characterized using Fourier transform infrared (FTIR) spectroscopy, ellipsometric porosimetry, X-ray photoelectron spectroscopy (XPS), and photoluminescence spectroscopy. It was observed that Eu doping made the films more hydrophilic and reduced the pore size and open porosity. The reduction from Eu^{3+} to Eu^{2+} occurred within the pores of the OSG films, as confirmed by depth profiling XPS. Eu^{3+} was found only on the top surface of the films. The presence of both Eu^{3+} and Eu^{2+} resulted in characteristic luminescence emission in the range of 600–630 nm (Eu^{3+}) and 300–400 nm. The ratio of Eu^{2+}/Eu^{3+} concentrations depended on the concentration of CH_3 groups in the films. Furthermore, the concentration of Eu^{2+} ions within the pores could be reduced through oxidation during exposure to inductively coupled plasma (ICP) oxygen plasma.

One intriguing observation is the shift of the photoluminescence (PL) spectra towards the low wavelength region (290–400 nm) in comparison to other Eu-doped silica-based materials such as xerogel, sputter-deposited SiCOH, and PMO that show luminescence in the range of 400–500 nm. This shift is likely attributed to the effects of energy transfer occurring between the host materials and the Eu^{2+} ions. While we currently lack sufficient data to fully elucidate the mechanism of energy transfer between the PMO matrix and Eu^{2+}, it is worth noting that the ability to shift the PL spectra towards the UV/blue region using well-defined silica-based materials holds significant importance in the development of light sources with controllable spectra.

Supplementary Materials: The following supporting information can be downloaded at the website of this paper posted on Preprints.org, Estimations of atomic concentration of Eu (at% of Eu).

Author Contributions: Conceptualization, M.R.B.; data curation, M.R., J.Z. (Jing Zhang), and A.S.V.; formal analysis, M.R., J.Z. (Jinming Zhang); funding acquisition, A.S.V., J.Z. (Jing Zhang) and M.R.B.; investigation, M.R.B.; methodology, M.R., J.Z. (Jinming Zhang), A.S.V.; project administration, J.Z. (Jing Zhang) and M.R.B.; resources, J.Z. (Jing Zhang); supervision, J.Z. (Jing Zhang) and M.R.B.; validation, M.R., J.Z. (Jinming Zhang) and A.S.V. and M.R.B.; visualization, M.R.; writing: original draft, M.R. and M.R.B.; writing: review & editing, M.R., A.S.V. and M.R.B. All authors have read and agreed to the published version of the manuscript.

Funding: This research was funded by R&D Program of Beijing Municipal Education Commission, grant number KZ202210009014. The APC was funded by R&D Program of the Beijing Municipal Education Commission and by Russian Science Foundation, grant number 23–79–30016.

Institutional Review Board Statement: The study do not require ethical approval.

Informed Consent Statement: Not applicable.

Data Availability Statement: The data presented in this study are available on request from the corresponding author.

Acknowledgments: It is our pleasure to thank S. Naumov (IOM Leipzig), A. Kabansky (LAM Research), A. Rybaltovsky and Yu. Mankelevich (Moscow State University) for valuable discussions and advices.

Conflicts of Interest: The authors declare no conflict of interest.

References

1. Zhou, Z.; Yin, B.; Michel, J. On-chip light sources for silicon photonics. *Light Sci. Appl.* **2015**, *4*, e358–e358, doi:10.1038/lsa.2015.131.
2. Boninelli, S.; Bellocchi, G.; Franzò, G.; Miritello, M.; Iacona, F. New strategies to improve the luminescence efficiency of Eu ions embedded in Si-based matrices. *J. Appl. Phys.* **2013**, *113*, 143503, doi:10.1063/1.4799407.
3. Bellocchi, G.; Fabbri, F.; Miritello, M.; Iacona, F.; Franzò, G. Multicolor Depth-Resolved Cathodoluminescence from Eu-Doped SiOC Thin Films. *ACS Appl. Mater. Interfaces* **2015**, *7*, 18201–18205, doi:10.1021/acsami.5b05348.
4. Gallis, S.; Nikas, V.; Kaloyeros, A.E. Silicon Oxycarbide Thin films and Nanostructures: Synthesis, Properties and Applications. In *Modern Technologies for Creating the Thin-film Systems and Coatings*; InTech, 2017.
5. Prucnal, S.; Sun, J.M.; Skorupa, W.; Helm, M. Switchable two-color electroluminescence based on a Si metal-oxide-semiconductor structure doped with Eu. *Appl. Phys. Lett.* **2007**, *90*, doi:10.1063/1.2735285.
6. Nazarov, A.N.; Tiagulskyi, S.I.; Tyagulskyy, I.P.; Lysenko, V.S.; Rebohle, L.; Lehmann, J.; Prucnal, S.; Voelskow, M.; Skorupa, W. The effect of rare-earth clustering on charge trapping and electroluminescence

Preprints (www.preprints.org) | NOT PEER-REVIEWED | Posted: 31 July 2023 doi:10.20944/preprints202307.2068.v1

in rare-earth implanted metal-oxide-semiconductor light-emitting devices. *J. Appl. Phys.* **2010**, *107*, doi:10.1063/1.3436591.
7. Rebohle, L.; Lehmann, J.; Prucnal, S.; Kanjilal, A.; Nazarov, A.; Tyagulskii, I.; Skorupa, W.; Helm, M. Blue and red electroluminescence of Europium-implanted metal-oxide-semiconductor structures as a probe for the dynamics of microstructure. *Appl. Phys. Lett.* **2008**, *93*, doi:10.1063/1.2964176.
8. Li, D.; Zhang, X.; Jin, L.; Yang, D. Structure and luminescence evolution of annealed Europium-doped silicon oxides films. *Opt. Express* **2010**, *18*, 27191, doi:10.1364/OE.18.027191.
9. Bellocchi, G.; Franzò, G.; Boninelli, S.; Miritello, M.; Cesca, T.; Iacona, F.; Priolo, F. Structural and luminescence properties of undoped and Eu-doped SiOC thin films. *IOP Conf. Ser. Mater. Sci. Eng.* **2014**, *56*, 012009, doi:10.1088/1757-899X/56/1/012009.
10. Blasse, G.; Grabmaier, B.C. *Luminescent Materials*; Springer Berlin Heidelberg: Berlin, Heidelberg, 1994; ISBN 978-3-540-58019-5.
11. Gaft, M.; Reisfeld, R.; Panczer, G. Interpretation of Luminescence Centers. In; 2015; pp. 221–420.
12. Kumar, G. B., Raoa, B. V., Babub, B. C., Hungerford, G., Nandyala, S. H. and Santos, J.D. Luminescence and energy transfer phenomena in lanthanide ions doped phosphor and glassy materials. In; Nandyala, S.H., Ed.; Materials Research Forum LLC., 2017; pp. 159–189.
13. Stojadinović, S.; Vasilić, R. Eu^{2+} photoluminescence in Al2O3 coatings obtained by plasma electrolytic oxidation. *J. Lumin.* **2018**, *199*, 240–244, doi:10.1016/j.jlumin.2018.03.062.
14. Baklanov, M.R.; Ho, P.S.; Zschech, E. *Advanced Interconnects for ULSI Technology*; Baklanov, M.R., Ho, P.S., Zschech, E., Eds.; John Wiley & Sons, Ltd: Chichester, UK, 2012; ISBN 9781119963677.
15. Grill, A.; Gates, S.M.; Ryan, T.E.; Nguyen, S. V.; Priyadarshini, D. Progress in the development and understanding of advanced low k and ultralow k dielectrics for very large-scale integrated interconnects - State of the art. *Appl. Phys. Rev.* **2014**, *1*, 011306, doi:10.1063/1.4861876.
16. Volksen, W.; Miller, R.D.; Dubois, G. Low Dielectric Constant Materials. *Chem. Rev.* **2010**, *110*, 56–110, doi:10.1021/cr9002819.
17. Goethals, F.; Ciofi, I.; Madia, O.; Vanstreels, K.; Baklanov, M.R.; Detavernier, C.; Van Der Voort, P.; Van Driessche, I. Ultra-low-k cyclic carbon-bridged PMO films with a high chemical resistance. *J. Mater. Chem.* **2012**, *22*, 8281, doi:10.1039/c2jm30312d.
18. Vishnevskiy, A.S.; Naumov, S.; Seregin, D.S.; Wu, Y.H.; Chuang, W.T.; Rasadujjaman, M.; Zhang, J.; Leu, J.; Vorotilov, K.A.; Baklanov, M.R. Effects of methyl terminal and carbon bridging groups ratio on critical properties of porous organosilicate-glass films. *Materials (Basel).* **2020**, *13*, 1–21, doi:10.3390/ma13204484.
19. Li, H.; Knaup, J.M.; Kaxiras, E.; Vlassak, J.J. Stiffening of organosilicate glasses by organic cross-linking. *Acta Mater.* **2011**, *59*, 44–52, doi:10.1016/j.actamat.2010.08.015.
20. Vanstreels, K.; Wu, C.; Gonzalez, M.; Schneider, D.; Gidley, D.; Verdonck, P.; Baklanov, M.R. Effect of Pore Structure of Nanometer Scale Porous Films on the Measured Elastic Modulus. *Langmuir* **2013**, *29*, 12025–12035, doi:10.1021/la402383g.
21. Kaczmarek, A.M.; Van Der Voort, P. Light-emitting lanthanide periodic mesoporous organosilica (PMO) hybrid materials. *Materials (Basel).* **2020**, *13*, doi:10.3390/ma13030566.
22. Lu, Y.; Fan, H.; Doke, N.; Loy, D.A.; Assink, R.A.; LaVan, D.A.; Brinker, C.J. Evaporation-Induced Self-Assembly of Hybrid Bridged Silsesquioxane Film and Particulate Mesophases with Integral Organic Functionality. *J. Am. Chem. Soc.* **2000**, *122*, 5258–5261, doi:10.1021/ja9935862.
23. Baklanov, M.R.; Mogilnikov, K.P.; Polovinkin, V.G.; Dultsev, F.N. Determination of pore size distribution in thin films by ellipsometric porosimetry. *J. Vac. Sci. Technol. B Microelectron. Nanom. Struct.* **2000**, *18*, 1385–1391, doi:10.1116/1.591390.
24. Baklanov, M. R., Mogilnikov, K. P. Mogilnikov, Vishnevskiy, A.S. Challenges in porosity characterization of thin films: cross-evaluation of different techniques. *J. Vac. Sci. Technol. A* **2023**.
25. Grill, A.; Neumayer, D.A. Structure of low dielectric constant to extreme low dielectric constant SiCOH films: Fourier transform infrared spectroscopy characterization. *J. Appl. Phys.* **2003**, *94*, 6697–6707, doi:10.1063/1.1618358.
26. Marsik, P.; Verdonck, P.; De Roest, D.; Baklanov, M.R. Porogen residues detection in optical properties of low-k dielectrics cured by ultraviolet radiation. *Thin Solid Films* **2010**, *518*, 4266–4272, doi:10.1016/j.tsf.2009.12.110.
27. ALOthman, Z. A Review: Fundamental Aspects of Silicate Mesoporous Materials. *Materials (Basel).* **2012**, *5*, 2874–2902, doi:10.3390/ma5122874.
28. Lowell, S.; Shields, J.E.; Thomas, M.A.; Thommes, M. *Characterization of Porous Solids and Powders: Surface Area, Pore Size and Density*; Particle Technology Series; Springer Netherlands: Dordrecht, 2004; Vol. 16; ISBN 978-90-481-6633-6.
29. Esquivel, D.; Kaczmarek, A.M.; Jiménez-Sanchidrián, C.; Van Deun, R.; Romero-Salguero, F.J.; Van Der Voort, P. Eu^{3+} @PMO: synthesis, characterization and luminescence properties. *J. Mater. Chem. C* **2015**, *3*, 2909–2917, doi:10.1039/C4TC02553A.

Preprints (www.preprints.org) | NOT PEER-REVIEWED | Posted: 31 July 2023 doi:10.20944/preprints202307.2068.v1

30. Li, Y.; Zhang, C.; Hu, H.; Wang, J.; Wang, X. Novel photoactive lanthanide hybrids covalently grafted on functionalized periodic mesoporous organosilicons (PMOs) by Schiff-base derivative. *J. Porous Mater.* **2017**, *24*, 487–496, doi:10.1007/s10934-016-0284-y.
31. Sheng, G.; Dong, H.; Shen, R.; Li, Y. Microscopic insights into the temperature-dependent adsorption of Eu(III) onto titanate nanotubes studied by FTIR, XPS, XAFS and batch technique. *Chem. Eng. J.* **2013**, *217*, 486–494, doi:10.1016/j.cej.2012.10.076.
32. Bilewska, K.; Wolna, E.; Edely, M.; Ruello, P.; Szade, J. $EuNiO_3$ thin films- growth and characterization. *J. Phys. Conf. Ser.* **2011**, *289*, 012014, doi:10.1088/1742-6596/289/1/012014.
33. Guo, X.; Jakes, J.E.; Banna, S.; Nishi, Y.; Shohet, J.L. Effects of plasma and vacuum-ultraviolet exposure on the mechanical properties of low-k porous organosilicate glass. *J. Appl. Phys.* **2014**, *116*, doi:10.1063/1.4891501.
34. Rasadujjaman, M.; Zhang, J.; Spassky, D.A.; Naumov, S.; Vishnevskiy, A.S.; Vorotilov, K.A.; Yan, J.; Zhang, J.; Baklanov, M.R. UV-Excited Luminescence in Porous Organosilica Films with Various Organic Components. *Nanomaterials* **2023**, *13*, 1419, doi:10.3390/nano13081419.
35. Wan, N.; Xu, J.; Lin, T.; Zhang, X.; Xu, L. Energy transfer and enhanced luminescence in metal oxide nanoparticle and rare earth codoped silica. *Appl. Phys. Lett.* **2008**, *92*, doi:10.1063/1.2936842.
36. Blasse, G., Dirksen, G. J., Van Vliet, J.P.M. The luminescence of Europium nitrate Hexahydrate, $Eu(NO_3)_3 \cdot 6H_2O$. *Inorganica Chim. Acta* **1988**, *142*, 165–168.
37. Lu, Q.; Wang, Z.; Wang, P.; Li, J. Structure and Luminescence Properties of Eu^{3+}-Doped Cubic Mesoporous Silica Thin Films. *Nanoscale Res. Lett.* **2010**, *5*, 761–768, doi:10.1007/s11671-010-9554-9.
38. Liu, W.; Kaczmarek, A.M.; Van Der Voort, P.; Van Deun, R. Chemical sensors based on periodic mesoporous organosilica @NaYF 4 :Ln^{3+} nanocomposites. *Dalt. Trans.* **2022**, *51*, 11467–11475, doi:10.1039/D2DT01469F.
39. Mulder, J.T.; Meijer, M.S.; van Blaaderen, J.J.; du Fossé, I.; Jenkinson, K.; Bals, S.; Manna, L.; Houtepen, A.J. Understanding and Preventing Photoluminescence Quenching to Achieve Unity Photoluminescence Quantum Yield in Yb:YLF Nanocrystals. *ACS Appl. Mater. Interfaces* **2023**, *15*, 3274–3286, doi:10.1021/acsami.2c17888.
40. Fneich, H.; Gaumer, N.; Chaussedent, S.; Blanc, W.; Mehdi, A. Europium-Doped Sol-Gel SiO_2-Based Glasses: Effect of the Europium Source and Content, Magnesium Addition and Thermal Treatment on Their Photoluminescence Properties. *Molecules* **2018**, *23*, 1768, doi:10.3390/molecules23071768.
41. Sipina, E. V.; Spassky, D.A.; Krutyak, N.R.; Morozov, V.A.; Zhukovskaya, E.S.; Belik, A.A.; Manylov, M.S.; Lazoryak, B.I.; Deyneko, D. V. Abnormal $Eu^{3+} \rightarrow Eu^{2+}$ Reduction in $Ca_{9-x}Mn_xEu(PO_4)_7$ Phosphors: Structure and Luminescent Properties. *Materials (Basel).* **2023**, *16*, 1383, doi:10.3390/ma16041383.
42. Maex, K.; Baklanov, M.R.; Shamiryan, D.; Lacopi, F.; Brongersma, S.H.; Yanovitskaya, Z.S. Low dielectric constant materials for microelectronics. *J. Appl. Phys.* **2003**, *93*, 8793–8841, doi:10.1063/1.1567460.
43. Ishizaka, T.; Nozaki, R.; Kurokawa, Y. Luminescence properties of Tb^{3+} and Eu^{3+}-doped alumina films prepared by sol-gel method under various conditions and sensitized luminescence. *J. Phys. Chem. Solids* **2002**, *63*, 613–617, doi:10.1016/S0022-3697(01)00201-3.
44. Yu, M.; Lin, J.; Fu, J.; Zhang, H.J.; Han, Y.C. Sol–gel synthesis and photoluminescent properties of LaPO 4 :A (A = Eu^{3+} , Ce^{3+} , Tb^{3+}) nanocrystalline thin films. *J. Mater. Chem.* **2003**, *13*, 1413–1419, doi:10.1039/B302600K.
45. Jia, W.; Liu, H.; Felofilov, S.P.; Meltzer, R.; Jiao, J. Spectroscopic study of Eu^{3+}-doped and Eu^{3+},Y^{3+}-codoped SiO_2 sol–gel glasses. *J. Alloys Compd.* **2000**, *311*, 11–15, doi:10.1016/S0925-8388(00)00850-1.
46. Baklanov, M.R.; De Marneffe, J.F.; Shamiryan, D.; Urbanowicz, A.M.; Shi, H.; Rakhimova, T. V.; Huang, H.; Ho, P.S. Plasma processing of low-k dielectrics. *J. Appl. Phys.* **2013**, *113*, doi:10.1063/1.4765297.
47. Braginsky, O. V.; Kovalev, A.S.; Lopaev, D. V.; Malykhin, E.M.; Mankelevich, Y.A.; Rakhimova, T. V.; Rakhimov, A.T.; Vasilieva, A.N.; Zyryanov, S.M.; Baklanov, M.R. The mechanism of low-k SiOCH film modification by oxygen atoms. *J. Appl. Phys.* **2010**, *108*, doi:10.1063/1.3486084.
48. Zhang, Y.; Li, X.; Li, K.; Lian, H.; Shang, M.; Lin, J. Crystal-Site Engineering Control for the Reduction of Eu 3+ to Eu^{2+} in $CaYAlO_4$: Structure Refinement and Tunable Emission Properties. *ACS Appl. Mater. Interfaces* **2015**, *7*, 2715–2725, doi:10.1021/am508859c.
49. Dereń, P.J.; Stefańska, D.; Ptak, M.; Wiśniewski, P. Method to Measure the Degree of Reduction of Eu^{3+} to Eu^{2+}: How Anion and Cation Vacancies Influence the Degree of Reduction. *J. Phys. Chem. C* **2021**, *125*, 24505–24514, doi:10.1021/acs.jpcc.1c06977.
50. Zaitoun, M.A.; Kim, T.; Lin, C.T. Observation of Electron−Hole Carrier Emission in the Eu^{3+}-Doped Silica Xerogel. *J. Phys. Chem. B* **1998**, *102*, 1122–1125, doi:10.1021/jp972536l.
51. Zaitoun, M.A.; Goken, D.M.; Bailey, L.S.; Kim, T.; Lin, C.T. Thermoanalysis and Emission Properties of Eu^{3+} /Eu^{2+} in Eu^{3+} -Doped Xerogels. *J. Phys. Chem. B* **2000**, *104*, 189–196, doi:10.1021/jp991873m.
52. He, J.; Wang, Y.; Liu, Y.; Wang, K.; Li, R.; Fan, J.; Xu, S.; Zhang, L. Tailoring the Luminescence of Europium Ions in Mesoporous $AlPO_4$ Monolithic Glass. *J. Phys. Chem. C* **2013**, *117*, 21916–21922, doi:10.1021/jp407125e.

Preprints (www.preprints.org) | NOT PEER-REVIEWED | Posted: 31 July 2023 doi:10.20944/preprints202307.2068.v1

53. Zhang, Q.; Qiao, Y.; Qian, B.; Dong, G.; Ruan, J.; Liu, X.; Zhou, Q.; Chen, Q.; Qiu, J.; Chen, D. Luminescence properties of the Eu-doped porous glass and spontaneous reduction of Eu^{3+} to Eu^{2+}. *J. Lumin.* **2009**, *129*, 1393–1397, doi:10.1016/j.jlumin.2009.07.013.
54. Biswas, A.; Friend, C.S.; Prasad, P.N. Spontaneous reduction of Eu^{3+} ion in Al co-doped sol–gel silica matrix during densification. *Mater. Lett.* **1999**, *39*, 227–231, doi:10.1016/S0167-577X(99)00011-7.
55. Wang, C.; Peng, M.; Jiang, N.; Jiang, X.; Zhao, C.; Qiu, J. Tuning the Eu luminescence in glass materials synthesized in air by adjusting glass compositions. *Mater. Lett.* **2007**, *61*, 3608–3611, doi:10.1016/j.matlet.2006.11.133.
56. Zhang, D.; Hu, X.; Jing, G.; Liu, E.; Fan, J.; Zhang, G.; Hou, X. Transition from Eu^{3+} to Eu^{2+} in SiO_2 Matrix Prepared by Sol–Gel. *J. Nanosci. Nanotechnol.* **2014**, *14*, 3642–3647, doi:10.1166/jnn.2014.8023.
57. Jousseaume, V.; Zenasni, A.; Gourhant, O.; Favennec, L.; R., B.M. Ultra-Low-k by CVD: Deposition and Curing. In *Advanced Interconnects for ULSI Technology*; Baklanov, M.R., Ho, P.S., Zschech, E., Eds.; John Wiley & Sons., Ltd.: UK, 2012 ISBN 9781119963677.
58. Palov, A.; Rakhimova, T. V.; Krishtab, M.B.; Baklanov, M.R. Dependence of dielectric constant of SiOCH low-k films on porosity and pore size. *J. Vac. Sci. Technol. B, Nanotechnol. Microelectron. Mater. Process. Meas. Phenom.* **2015**, *33*, 020603, doi:10.1116/1.4906816.
59. Kumar, B.P.; Kumar, A.P.; Bindu, P.H.; Mukherjee, A.K.; Patra, A.S. Red Light Emission of POSS Triol Chelated with Europium. *Asian J. Nanosci. Mater.* **2019**, *2*, 244–256, doi:10.26655/ajnanomat.2019.3.10.
60. Horrocks, W.D.; Schmidt, G.F.; Sudnick, D.R.; Kittrell, C.; Bernheim, R.A. Laser-induced lanthanide ion luminescence lifetime measurements by direct excitation of metal ion levels. A new class of structural probe for calcium-binding proteins and nucleic acids. *J. Am. Chem. Soc.* **1977**, *99*, 2378–2380, doi:10.1021/ja00449a079.
61. Dorenbos, P. Energy of the first $4f^7 \rightarrow 4f^6 5d$ transition of Eu^{2+} in inorganic compounds. *J. Lumin.* **2003**, *104*, 239–260, doi:10.1016/S0022-2313(03)00078-4.

Disclaimer/Publisher's Note: The statements, opinions and data contained in all publications are solely those of the individual author(s) and contributor(s) and not of MDPI and/or the editor(s). MDPI and/or the editor(s) disclaim responsibility for any injury to people or property resulting from any ideas, methods, instructions or products referred to in the content.